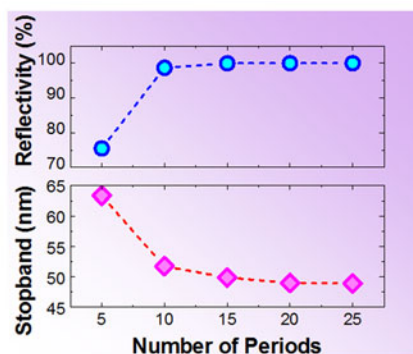
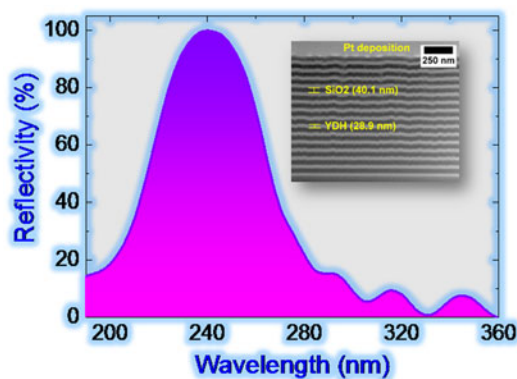


# High Reflectivity YDH/SiO<sub>2</sub> Distributed Bragg Reflector for UV-C Wavelength Regime

Volume 10, Number 2, April 2018








Mohd Sharizal Alias, *Member, IEEE*  
Abdullah A. Alatawi  
Wong Kim Chong  
Malleswararao Tangi  
Jorge A. Holguin-Lerma, *Student Member, IEEE*  
Edgars Stegenburgs  
Mohammad Khaled Shakfa  
Tien Khee Ng, *Senior Member, IEEE*  
Abdulrahman M. Albadri  
Ahmed Y. Alyamani  
Boon S. Ooi, *Senior Member, IEEE*



DOI: 10.1109/JPHOT.2018.2804355

1943-0655 © 2018 IEEE

# High Reflectivity YDH/SiO<sub>2</sub> Distributed Bragg Reflector for UV-C Wavelength Regime

Mohd Sharizal Alias <sup>1</sup>, Member, IEEE, Abdullah A. Alatawi <sup>1,3</sup>,  
Wong Kim Chong,<sup>2</sup> Malleswararao Tangi,<sup>1</sup>  
Jorge A. Holguin-Lerma <sup>1</sup>, Student Member, IEEE,  
Edgars Stegenburgs <sup>1</sup>, Mohammad Khaled Shakfa <sup>1</sup>,  
Tien Khee Ng <sup>1</sup>, Senior Member, IEEE, Abdulrahman M. Albadri,<sup>3</sup>  
Ahmed Y. Alyamani,<sup>3</sup> and Boon S. Ooi <sup>1</sup>, Senior Member, IEEE

<sup>1</sup>Photonics Laboratory, Computer, Electrical and Mathematical Science and Engineering Division, King Abdullah University of Science and Technology, Thuwal 23955-6900, Saudi Arabia

<sup>2</sup>Core Labs, King Abdullah University of Science and Technology, Thuwal 23955-6900, Saudi Arabia

<sup>3</sup>National Center for Nanotechnology, King Abdulaziz City for Science and Technology, Riyadh 11442-6086, Saudi Arabia

DOI:10.1109/JPHOT.2018.2804355

1943-0655 © 2018 IEEE. Translations and content mining are permitted for academic research only. Personal use is also permitted, but republication/redistribution requires IEEE permission. See [http://www.ieee.org/publications\\_standards/publications/rights/index.html](http://www.ieee.org/publications_standards/publications/rights/index.html) for more information.

Manuscript received December 25, 2017; revised January 24, 2018; accepted February 6, 2018. Date of publication February 12, 2018; date of current version March 1, 2018. This paper is based on the work supported in part by the King Abdulaziz City for Science and Technology under Grant KACST TIC R2-FP-008, and in part by the King Abdullah University of Science and Technology baseline funding BAS/1/1614-01-01. Corresponding author: B. S. Ooi (e-mail: boon.ooi@kaust.edu.sa).

**Abstract:** A distributed Bragg reflector (DBR) composed of Y<sub>2</sub>O<sub>3</sub>-doped HfO<sub>2</sub> (YDH)/SiO<sub>2</sub> layers with high reflectivity spectrum centered at a wavelength of ~240 nm is fabricated using radio-frequency magnetron sputtering. Before the DBR deposition, optical properties for a single layer of YDH, SiO<sub>2</sub>, and HfO<sub>2</sub> thin films were studied using spectroscopic ellipsometry and spectrophotometry. To investigate the performance of YDH as a material for the high refractive index layer in the DBR, a comparison of its optical properties was made with HfO<sub>2</sub> thin films. Due to larger optical bandgap, the YDH thin films demonstrated higher transparency, lower extinction coefficient, and lower absorption coefficient in the UV-C regime (especially for wavelengths below 250 nm) compared to the HfO<sub>2</sub> thin films. The fabricated YDH/SiO<sub>2</sub> DBR consisting of 15 periods achieved a reflectivity higher than 99.9% at the wavelength of ~240 nm with a stopband of ~50 nm. The high reflectivity and broad stopband of YDH/SiO<sub>2</sub> DBRs will enable further advancement of various photonic devices such as vertical-cavity surface-emitting lasers, resonant-cavity light-emitting diodes, and resonant-cavity photodetectors operating in the UV-C wavelength regime.

**Index Terms:** Distributed Bragg reflector, thin films, ultraviolet.

## 1. Introduction

Highly reflective distributed Bragg reflectors (DBRs) in the ultraviolet (UV) wavelength regime are important for UV-based photonic devices such as vertical-cavity surface-emitting lasers (VCSELs), polariton lasers, light-emitting diodes (LEDs), photodetectors (PDs), and solar cells. DBRs can be integrated into these devices as mirrors to enhance the light amplification. Typically, a DBR

can be formed by repetitively stacking alternating high- and low-refractive index (RI) layers with the thickness of each layer corresponding to a quarter-wave of the operating wavelength. In the UV wavelength regime, group III-nitride materials (e.g., GaN/AlGa<sub>N</sub>, AlGa<sub>N</sub>/AlIn<sub>N</sub>, AlGa<sub>N</sub>/AlN, and AlGa<sub>N</sub>/air), and dielectric materials (e.g., TiO<sub>2</sub>/SiO<sub>2</sub>, Ta<sub>2</sub>O<sub>5</sub>/SiO<sub>2</sub>, HfO<sub>2</sub>/SiO<sub>2</sub>, and ZrO<sub>2</sub>/SiO<sub>2</sub>) based-DBRs have been used in the design and fabrication of UV VCSEL [1]–[3], UV edge-emitting laser [4], UV polariton laser [5], UV resonant-cavity LED [6], UV LED [7], and UV PD [8]. The advantages of group III-nitride DBRs is that they can be monolithically grown and doped with desired n- or p-type dopants required for electrical pumping. However, obtaining dislocation- and crack-free structures is challenging due to the limited crystal quality (e.g., lattice- and thermal expansion-mismatch), growth complexity (e.g., composition- and growth temperature-fluctuation), and the inadequate reflectivity (i.e., low RI contrast) of group III-nitride materials. In contrast, for dielectric DBRs, the choice of the materials and the growth method are more extensive and flexible. Highly reflective DBRs exceeding 99% reflectivity can be easily obtained within a small number of repetitions due to the high RI contrast, i.e., 10 to 15 periods typically [2], [5], compared to 30 to 50 periods for group III-nitride DBRs [9]. However, a complex device scheme, e.g., the intra-cavity design, is required to realize electrical pumping for devices using dielectric DBRs [6].

Focusing on dielectric DBRs for the UV-C regime i.e., <280 nm wavelength, the use of fluorides, e.g., LaF<sub>3</sub>/AlF<sub>3</sub> [10] and LaF<sub>3</sub>/MgF<sub>2</sub> [11]; oxide-fluoride combinations, e.g., Al<sub>2</sub>O<sub>3</sub>/MgF<sub>2</sub> [12] and Al<sub>2</sub>O<sub>3</sub>/AlF<sub>3</sub> [10]; and oxides only, e.g., Al<sub>2</sub>O<sub>3</sub>/SiO<sub>2</sub> [13] and HfO<sub>2</sub>/SiO<sub>2</sub> [14], [15]; have been reported. The fluorides and oxides-fluorides based DBRs were developed for reflectivities at sub-200 nm wavelengths [10]–[12]. For operating wavelengths above 200 nm, the oxides based DBRs were used [13]–[16]. Although fluorides exhibit relatively low UV-C absorption, a high number (>40 pairs) of DBR periods is required due to the small RI contrast [10]. Furthermore, fluoride layers are required to be deposited at high substrate temperature to obtain stable film structural and optical properties. This condition promotes high tensile stress during the deposition due to the large thermal expansion coefficient difference between the film and the substrate, which can lead to micro-cracks for a thick DBR structure [10]. If using oxides only as in the case of Al<sub>2</sub>O<sub>3</sub>/SiO<sub>2</sub> DBR [13], around 42.5 periods were required to achieve a reflectivity of >99% in the UV-C regime due to insufficient RI contrast. Replacing Al<sub>2</sub>O<sub>3</sub> by HfO<sub>2</sub> as the high RI layer for the DBR (with SiO<sub>2</sub> as the low RI layer) is attractive because of higher RI contrast. However, HfO<sub>2</sub> starts absorbing light below the wavelength of 250 nm. Therefore, most of the reported HfO<sub>2</sub>/SiO<sub>2</sub> DBRs have been only designed for wavelengths above 250 nm [13]–[16]. Recently, it has been shown that the material properties of HfO<sub>2</sub> films can be improved by the incorporation of Y<sub>2</sub>O<sub>3</sub> (also known as yttria). Compared with HfO<sub>2</sub> films, the Y<sub>2</sub>O<sub>3</sub>-doped HfO<sub>2</sub> (YDH) films exhibited better structural stability [17], [18], higher effective dielectric constant [19], lower leakage current density [17], and larger optical bandgap [20]–[22]. Specifically, on the optical bandgap ( $E_g$ ), Noor-A-Alam *et al.* [20] and Chen *et al.* [21], [22] reported that more than 6 eV could be achieved for YDH films with a certain composition.

Here, we demonstrate a YDH/SiO<sub>2</sub> DBR with a reflectivity higher than 99.9% operating in the UV-C regime. This DBR exhibits a ~50 nm broad stopband centered at ~240 nm wavelength. Due to the high RI contrast and low absorption of the materials, the YDH/SiO<sub>2</sub> DBR requires only 15 periods to achieve the aforementioned reflectivity. We also compare the optical characteristics of single layer YDH and HfO<sub>2</sub> thin films prior to the full DBR deposition. Recently, several AlGa<sub>N</sub>-based lasers were reported for UV-C lasing at ~240 nm wavelength [23]–[26]. By having such as high reflectivity around 240 nm wavelength with only 15 periods, YDH/SiO<sub>2</sub> DBRs can be used as a mirror for these UV-C lasers and other UV-C photonic devices.

## 2. Depositions of DBRs and Thin Films

The YDH/SiO<sub>2</sub> DBRs were deposited onto UV-grade sapphire substrates by radio-frequency (RF) magnetron sputtering. A single layer of YDH, HfO<sub>2</sub>, and SiO<sub>2</sub> thin films were also deposited onto both UV-grade sapphire and silicon substrates to investigate the optical properties of these materials. All substrates were cleaned using the standard solvents-ultrasonic cleaning and dried with N<sub>2</sub> before being loaded into the vacuum chamber, which was initially evacuated to a base pressure

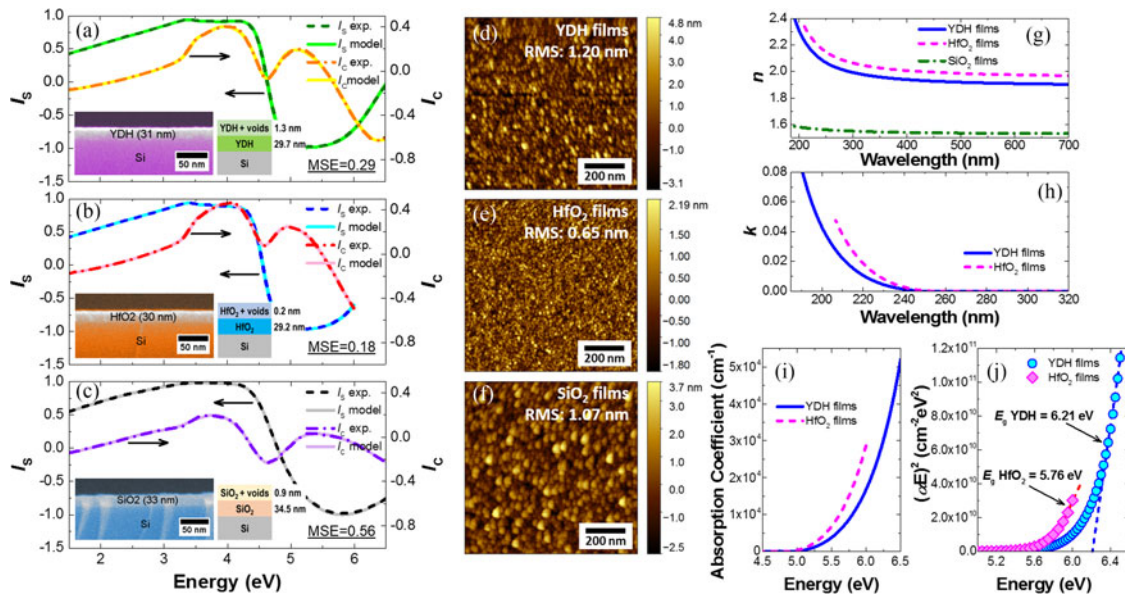


Fig. 1. Measurements and analysis of the YDH, HfO<sub>2</sub>, and SiO<sub>2</sub> thin films showing (a)–(c) modeled and experimentally obtained SE spectra of each material with the SEM cross-section micrograph (left) and optical stack model (right) as insets, (d)–(f) AFM surface scan for each material with the respective RMS roughness value, (g) wavelength-dependent RI spectra, (h) wavelength-dependent extinction coefficient spectra, (i) absorption coefficient spectra, and (j) Tauc plot revealing the values of optical bandgap.

of  $\sim 10^{-7}$  torr. A commercial-ready 2-inch diameter YDH target composed of (Y<sub>2</sub>O<sub>3</sub>)<sub>0.2</sub>(HfO<sub>2</sub>)<sub>0.8</sub>, SiO<sub>2</sub> target, and HfO<sub>2</sub> target with a purity of 99.9%, 99.995%, and 99.95%, respectively, were used for the sputtering. The RF power applied to all targets were set to 75 W. The sputtering gas was Ar with the gas flow maintained at 25 sccm. Before the actual deposition, all targets were pre-sputtered for 10 min with the shutter above the sputter gun closed. All samples were sputtered at room temperature with a working pressure of  $\sim 10^{-3}$  torr. The deposition rates were 2.4, 2.0, and 0.8 nm/min for HfO<sub>2</sub>, YDH, and SiO<sub>2</sub> thin films, respectively.

### 3. Material Characterizations of Thin Films

To design the YDH/SiO<sub>2</sub> DBR, measurements using spectroscopic ellipsometer (SE) were performed to investigate the wavelength-dependent RI ( $n$ ) of YDH and SiO<sub>2</sub> thin films, and to study the comparison of extinction coefficient ( $k$ ) and  $E_g$  between YDH and HfO<sub>2</sub> thin films in the UV regime. The deposited thickness of all samples was fixed to  $\sim 30$  nm. Since the wavelength of interest is in the UV regime, a phase modulated SE was used where the signals detected are in the form of harmonics (symbolized as  $I_s$  and  $I_c$ ) that can be extracted to determine the ellipsometric angles ( $\Psi$  and  $\Delta$ ) as a function of energy [27]. Data were acquired at an incident angle of 70° over a spectral range from 1.5 eV up to just beyond the respective  $E_g$  for each material. To extract the optical constants ( $n$  and  $k$ ), film thickness, and the surface morphology information, the measured harmonics were fitted to data generated from a model representing the sample structure. For the SE modeling, the Tauc-Lorentz model [28] (which is suited for amorphous semiconductors and Kramers-Kronig consistent) was used for the YDH, HfO<sub>2</sub>, and SiO<sub>2</sub> materials. A good fit to the measured data indicated by the lowest possible mean squared error (MSE) based on Levenberg-Marquardt regression algorithm is required across the measured spectral range. Fig. 1(a) to (c) show the measured versus modeled SE spectra with a good fitting obtained (nominal MSE values) for the YDH, HfO<sub>2</sub>, and SiO<sub>2</sub> thin films, respectively, and show the corresponding scanning electron microscope (SEM) cross-section micrographs and optical stack models in insets. The thickness of the single YDH, HfO<sub>2</sub>, and SiO<sub>2</sub> layers and the root-mean-square (RMS) roughness obtained from

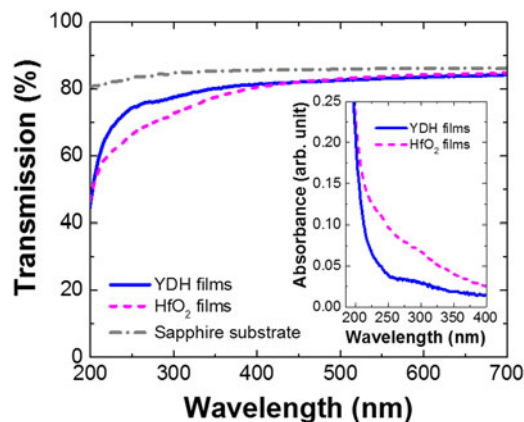


Fig. 2. Transmission spectra of the YDH and HfO<sub>2</sub> thin films deposited on UV-grade sapphire substrates. The inset shows the absorbance spectra for both materials in the UV regime.

the SE modeling were in good agreement with the measured cross-sectional micrographs using SEM and the surface scans using atomic force microscope (AFM). The AFM images for the YDH, HfO<sub>2</sub>, and SiO<sub>2</sub> thin films are shown in Fig. 1(d) to (f), respectively, for an area of  $1 \times 1 \mu\text{m}^2$ .

Fig. 1(g) and (h) exhibit the SE extracted wavelength-dependent optical constants ( $n$  and  $k$ ) for the YDH, HfO<sub>2</sub>, and SiO<sub>2</sub> thin films. It is found that  $n$  decreases slightly when Y<sub>2</sub>O<sub>3</sub> is doped to the HfO<sub>2</sub> material (i.e., YDH thin films). This can be attributed to oxygen vacancies (from Y<sub>2</sub>O<sub>3</sub>) incorporated into the HfO<sub>2</sub> lattice, resulting in a reduced material density and hence in the  $n$  value. At a wavelength of 350 nm, for comparison, the  $n$  values obtained here are in excellent agreement with the results from the literature [15], [22], [29], with only deviations of  $\pm 0.58\%$  for YDH,  $\pm 1.12\%$  for HfO<sub>2</sub>, and  $\pm 2.55\%$  for SiO<sub>2</sub> thin films. By using the measured  $k$  values of the YDH and HfO<sub>2</sub> thin films, the absorption coefficient,  $\alpha$  for each material is calculated [see Fig. 1(i)] from the following relation of  $\alpha = 4\pi k/\lambda$ . Subsequently, the  $E_g$  is estimated using the Tauc plot as shown in Fig. 1(j), and is found to be  $\sim 6.21$  and  $\sim 5.76$  eV for the YDH and HfO<sub>2</sub> thin films, respectively. The  $E_g$  value of the YDH thin films is consistent with the finding reported by Chen *et al.* which is  $\sim 6.24$  eV for (Y<sub>2</sub>O<sub>3</sub>)<sub>0.26</sub>(HfO<sub>2</sub>)<sub>0.74</sub> [22]. As for the HfO<sub>2</sub> thin films, the estimated  $E_g$  is comparable with various values reported in the literature [30]–[32]. It was assumed that the doping of Y<sub>2</sub>O<sub>3</sub> changes the chemical element, i.e., electron states (from Hf-O-Hf to Hf-O-Y) [21], and furthermore introduces charge defects that increase the  $E_g$  of HfO<sub>2</sub> material [33]. This has been shown using the first-principles calculation that by adding Y<sub>2</sub>O<sub>3</sub> to the HfO<sub>2</sub> material, the highest occupied defect level will fall into the valence band rather than the energy gap, which explains the  $E_g$  broadening [33]. The  $E_g$  can also be affected by the microstructure of the films. It has been shown that the degree of crystallinity for YDH thin films can be improved (from amorphous to polycrystalline) for  $>8\%$  doping of Y<sub>2</sub>O<sub>3</sub> into the HfO<sub>2</sub> material [21]. This can be examined from the AFM surface scans shown in Fig. 1(d) and (e) for the YDH and HfO<sub>2</sub> thin films, respectively. Irregular nanograins can be well observed on the YDH thin films which are correlated with an increase in the RMS roughness to  $\sim 1.20$  nm, compared to the RMS roughness of the HfO<sub>2</sub> thin films which is only  $\sim 0.65$  nm. The HfO<sub>2</sub> thin films exhibit more uniform surface, i.e., less and smaller nanograins, which is consistent with reported amorphous HfO<sub>2</sub> thin films (i.e., similar AFM image and RMS roughness  $\sim 0.91$  nm) [34]. A change in films microstructure can increase the  $E_g$ , as a similar behavior was observed in yttria-stabilized zirconia (YSZ) thin films [35]. Additionally, the increase in the lattice constant and the development of strain in YDH thin films can also increase the  $E_g$  [20].

The increase in  $E_g$  that results in lower  $\alpha$  and  $k$  values, indicates the transparency of the YDH films in the UV-C wavelengths below 250 nm. This is proven by comparing the transmission measurement of the YDH and HfO<sub>2</sub> thin films using spectrophotometer (see Fig. 2). Both materials were deposited at the same thickness of  $\sim 30$  nm on UV-grade sapphire substrates (thickness of  $\sim 430 \mu\text{m}$ ). The transparency of  $\sim 80\%$  in the visible regime exhibited by YDH and HfO<sub>2</sub> thin films is consistent

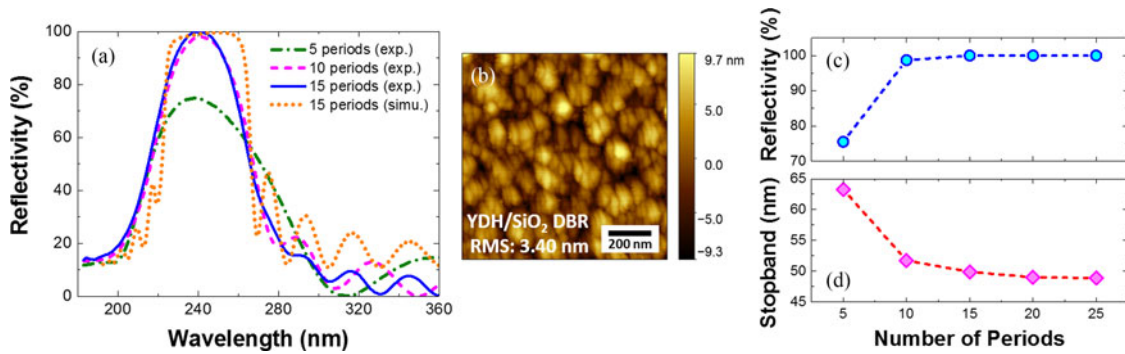


Fig. 3. YDH/SiO<sub>2</sub> DBR characteristics showing (a) experimental and simulated reflectivity spectra for various DBR periods, and (b) AFM surface scan for the DBR structure with 15 periods. The (c) reflectivity and (d) stopband for various DBR periods.

with the literature [21], [29], [30], [32], [36]. Focusing in the UV regime, the YDH thin films is more transparent compared to HfO<sub>2</sub> thin films. The absorbance spectrum (inset of Fig. 2) reveals that the YDH thin films only start absorbing drastically for wavelengths shorter than  $\sim 225$  nm. In comparison, the HfO<sub>2</sub> thin films already show apparent absorption even in the UV-A regime. Therefore, by doping Y<sub>2</sub>O<sub>3</sub> into the HfO<sub>2</sub> material, the newly formed YDH material is a promising candidate as the high RI layer for forming a UV-C dielectric DBR together with SiO<sub>2</sub> as the low RI layer. Although the  $n$  value for the YDH decreases slightly compared to HfO<sub>2</sub> [as shown in Fig. 1(g)], the RI contrast is still high. Other materials being used as the high RI layer for the oxide or fluoride type UV-C DBRs (e.g., Al<sub>2</sub>O<sub>3</sub> [10] and LaF<sub>3</sub> [13]) have even lower  $n$  values (>20% reduction). This resulted in insufficient RI contrast and thus a high number of periods (>40 periods) were required to achieve >99% reflectivity [13].

#### 4. Design and Characterizations of DBRs

Next, various YDH/SiO<sub>2</sub> DBRs were deposited on UV-grade sapphire substrates with a target center wavelength of 240 nm. The thickness of each layer in the DBR was designed at quarter-wavelength and the deposition was calibrated with SE measurements. The number of periods deposited was varied from 5 to 25 to compare the reflectivity and stopband of the DBR. The reflectivity measurements were performed using a spectrophotometer equipped with an integrating sphere and baselined with a UV certified MgF<sub>2</sub>-coated Al mirror. By applying the measured  $n$  and  $k$  values for each material, the transfer-matrix method (TMM) simulations were used to calculate the reflectivity spectrum and required layer thickness. The DBR stopband is approximated by [37]

$$\frac{\Delta\lambda}{\lambda_o} = \frac{4}{\pi} \arcsin\left(\frac{n_1 - n_2}{n_1 + n_2}\right) \quad (1)$$

where  $\lambda_o$  is the center wavelength,  $n_1$  is the high RI, and  $n_2$  is the low RI. Fig. 3(a) shows the experimental reflectivity spectra for YDH/SiO<sub>2</sub> DBRs of 5, 10 and 15 periods. The simulated reflectivity spectrum for 15 periods DBR is also shown for comparison. The reflectivity spectra of the experiment and simulation for YDH/SiO<sub>2</sub> DBR with 15 periods show good agreement in terms of the reflectivity peak and position of the spectrum. However, the stopband of the experimental spectrum is slightly narrower than in the simulation result. This might arise from a smaller RI contrast in the actual case when taking into account the optical loss from material absorption and interface scattering.

Fig. 3(b) shows the AFM surface scan of the 15 periods YDH/SiO<sub>2</sub> DBR. The RMS roughness is  $\sim 3.40$  nm, which is rougher than the single layer films of YDH and SiO<sub>2</sub> shown in Fig. 1. The increase in RMS roughness is associated with the interface roughness in the DBR stack, as evidenced in the cross-sectional SEM shown in the inset of Fig. 4. These imperfect interfaces can introduce

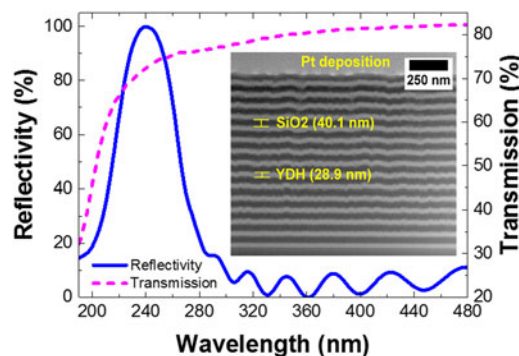


Fig. 4. The reflectivity spectrum for 15 periods YDH/SiO<sub>2</sub> DBR and the transmission spectrum for a  $\sim 29$  nm thick YDH thin films. The inset shows the cross-sectional SEM of the DBR structure.

scattering loss to the DBR, which can degrade the device performance (e.g., device efficiency of a VCSEL [38]). The absence of sideband interference fringes at shorter wavelength for the experiment spectra is due to the onset of the fundamental YDH absorption edge. Fig. 3(c) exhibits that a high reflectivity of  $>99.9\%$  can be achieved with only 15 periods of YDH/SiO<sub>2</sub> DBR. For comparison, more than 40 periods are required for Al<sub>2</sub>O<sub>3</sub>/SiO<sub>2</sub> DBR to achieve the same reflectivity in the UV-C regime due to insufficient RI contrast [13]. Due to the high RI contrast, the stopband of YDH/SiO<sub>2</sub> DBR is also considered broad (i.e.,  $\sim 50$  nm) as shown in Fig. 3(d), which can cover an extensive spectrum of the UV-C regime. If Al<sub>2</sub>O<sub>3</sub>/SiO<sub>2</sub> DBR is used, the stopband achieved is only  $\sim 26$  to  $39$  nm broad [13].

In Fig. 4, the reflectivity spectrum of 15 periods YDH/SiO<sub>2</sub> DBR is plotted with the transmission spectrum of single layer YDH thin films (thickness of a quarter-wavelength, i.e.,  $\sim 29$  nm). The reflectivity peak is obtained merely before the absorption of the YDH layers in the YDH/SiO<sub>2</sub> DBR becomes dominant. The inset of Fig. 4 shows the cross-sectional SEM micrograph of the DBR structure. The cross-sectional SEM sample was prepared using the focused-ion-beam (FIB) lift-out technique with Pt-coated on top as a protection layer during the FIB milling. The cross-sectional SEM shows a clear contrast between the individual YDH (bright) and SiO<sub>2</sub> (dark) layers. A homogeneous layer sequence showing uniform period thickness distribution along the growth direction (bottom-up) was observed. The thickness of the deposited YDH and SiO<sub>2</sub> thin films were highly precise and in excellent agreement ( $<1\%$  tolerance) with the thickness calculated from the TMM simulation. As the number of periods deposited for YDH/SiO<sub>2</sub> DBR increases, the interfaces were less smooth due to the accumulation of strain and the roughness introduced by each layer. This can potentially be improved by further optimization of the deposition process (e.g., RF power, Ar pressure, reactive sputtering of O<sub>2</sub>:Ar, and substrate temperature). For example, the RMS roughness decreased (from 2.97 to 2.10 nm) as the RF power was increased from 50 to 80 W during the sputtering of HfO<sub>2</sub> films [29]. Also, by using reactive sputtering (example mixing O<sub>2</sub>:Ar), the RMS roughness can be reduced. It is found that a smoother surface was obtained, i.e., RMS roughness reduced from 8.61 to 4.57 nm as the O<sub>2</sub>:Ar flow ratio increased from 0 to 0.2 for sputtered HfO<sub>2</sub> films [32]. All of the above approaches are applicable for minimizing the interface roughness during the sputtering of YDH/SiO<sub>2</sub> DBRs.

A summary of the key parameters achieved in this study is listed in Table 1. Compared with the prior reported work of other oxides-based DBRs, the YDH/SiO<sub>2</sub> DBR features the highest reflectivity at sub-250 nm operating wavelengths by using only 15 periods and demonstrates a broad stopband of  $\sim 50$  nm. By optimizing the deposition process as mentioned above, smoother interfaces can be obtained, and higher reflectivity for the DBR can be achieved with fewer period numbers. From the fabrication point of view, in addition to the RF magnetron sputtering, the DBRs (taking HfO<sub>2</sub>/SiO<sub>2</sub> DBR for example) can be fabricated using various deposition methods such as plasma ion-assisted deposition (PIAD) [15], ion plating (IP) [15], and ion-beam-assisted electron-gun vacuum evaporation [16]. Although the RI values change slightly for HfO<sub>2</sub> and SiO<sub>2</sub> when

TABLE 1  
Comparison of the Performance of Oxides-Based DBRs for UV Wavelengths

Material system	Fabrication method	Period	Center wavelength (nm)	Reflectivity (%)	Stopband (nm)	Ref.
Al <sub>2</sub> O <sub>3</sub> /SiO <sub>2</sub>	RF magnetron sputtering	42.5	296	99.0	26 to 39	[13]
HfO <sub>2</sub> /SiO <sub>2</sub>	RF magnetron sputtering	10	311	97.0	65	[13]
HfO <sub>2</sub> /SiO <sub>2</sub>	Plasma ion-assisted deposition	11.5	250	98.8	45	[15]
YDH/SiO <sub>2</sub>	<b>RF magnetron sputtering</b>	<b>15</b>	<b>240</b>	<b>99.9</b>	<b>50</b>	<b>This work</b>

PIAD and IP deposition methods are used [15], the RI deviations for both materials are still <10%. As above discussed, the RI value of our deposited YDH films (using RF magnetron sputtering) only deviates  $\pm 0.58\%$  compared to the RI values of YDH films deposited using electron beam evaporation [22]. To compensate any significant RI variation, additional period can be deposited for the DBR to obtain the targeted reflectivity. In addition to the RI, other DBR related factors such as thickness and interface roughness can be controlled through the optimization of the fabrication process. Reveret *et al.* [16] reported that as long as the interface roughness is <5 nm, the DBR reflectivity remain the same. Our AFM surface-scan indicates RMS roughness of  $\sim 3.40$  nm for the YDH/SiO<sub>2</sub> DBR. Moreover, the fabricated thickness is well-controlled (<1% fabrication tolerance) as shown from the cross-sectional SEM.

## 5. Conclusion

In summary, a highly reflective >99.9% oxides-based DBR was demonstrated for the UV-C wavelength regime by using 15 periods of YDH/SiO<sub>2</sub> layers. The reflectivity spectrum was centered at  $\sim 240$  nm with a relatively broad stopband of  $\sim 50$  nm. A comparison between YDH and HfO<sub>2</sub> thin films was made using the SE and spectrophotometry techniques. The YDH thin films exhibited better transparency in the UV-C regime especially below 250 nm, making this material promising as the high RI layer in a DBR structure. The realization of highly reflective and broad stopband YDH/SiO<sub>2</sub> DBR will benefit the UV photonic devices advancement for improved device efficiency in the UV-C regime.

## Acknowledgment

This research used resources of the Core Labs of KAUST.

## References

- [1] T. Someya, K. Tachibana, J. Lee, T. Kamiya, and Y. Arakawa, "Lasing emission from an In<sub>0.1</sub>Ga<sub>0.9</sub>N vertical cavity surface emitting laser," *Jpn. J. Appl. Phys.*, vol. 37, no. 12A, pp. L1424–L1426, 1998.
- [2] J. Y. Zhang *et al.*, "Blue-violet lasing of optically pumped GaN-based vertical cavity surface-emitting laser with dielectric distributed Bragg reflectors," *J. Lightw. Technol.*, vol. 27, no. 1, pp. 55–59, Jan. 2009.
- [3] Y.-S. Liu *et al.*, "Optically pumped vertical-cavity surface-emitting laser at 374.9 nm with an electrically conducting n-type distributed Bragg reflector," *Appl. Phys. Exp.*, vol. 9, no. 11, Oct. 2016, Art. no. 111002.
- [4] T. T. Kao *et al.*, "Sub-250 nm low-threshold deep-ultraviolet AlGaN-based heterostructure laser employing HfO<sub>2</sub>/SiO<sub>2</sub> dielectric mirrors," *Appl. Phys. Lett.*, vol. 103, no. 21, Nov. 2013, Art. no. 211103.
- [5] F. Li *et al.*, "Fabrication and characterization of a room-temperature ZnO polariton laser," *Appl. Phys. Lett.*, vol. 102, no. 19, May 2013, Art. no. 191118.



- [6] T. Moudakir *et al.*, "Design, fabrication, and characterization of near-milliwatt-power RCLEDs emitting at 390 nm," *IEEE Photon. J.*, vol. 5, no. 6, Dec. 2013, Art. no. 8400709.
- [7] M. S. Alias *et al.*, "Enhancing the light-extraction efficiency of an AlGaIn nanowire ultraviolet light-emitting diode by using nitride/air distributed Bragg reflector nanogratings," *IEEE Photon. J.*, vol. 9, no. 5, Oct. 2017, Art. no. 4900508.
- [8] Z. Xie *et al.*, "AlGaIn-based 330 nm resonant-cavity-enhanced p-i-n junction ultraviolet photodetectors using AlN/AlGaIn distributed Bragg reflectors," *Phys. Status Solidi C*, vol. 7, nos. 7–8, pp. 1821–1824, 2010.
- [9] T. Detchprohm *et al.*, "Sub 250 nm deep-UV AlGaIn/AlN distributed Bragg reflectors," *Appl. Phys. Lett.*, vol. 110, no. 1, Jan. 2017, Art. no. 011105.
- [10] J. Sun, X. Li, W. Zhang, K. Yi, and J. Shao, "High-reflectivity mirrors by Al<sub>2</sub>O<sub>3</sub>, LaF<sub>3</sub> and AlF<sub>3</sub> for 193 nm application," *Opt. Laser Technol.*, vol. 56, pp. 65–70, 2014.
- [11] F. Sarto *et al.*, "Vacuum-ultraviolet optical properties of ion beam assisted fluoride coatings for free electron laser applications," *Thin Solid Films*, vol. 515, no. 7, pp. 3858–3866, 2007.
- [12] S. Shuzhen, S. Jianda, L. Chunyan, Y. Kui, F. Zhengxiu, and C. Lei, "High-reflectance 193 nm Al<sub>2</sub>O<sub>3</sub>/MgF<sub>2</sub> mirrors," *Appl. Surf. Sci.*, vol. 249, no. 1, pp. 157–161, 2005.
- [13] M. L. Grilli, F. Menchini, A. Piegari, D. Alderighi, G. Toci, and M. Vannini, "Al<sub>2</sub>O<sub>3</sub>/SiO<sub>2</sub> and HfO<sub>2</sub>/SiO<sub>2</sub> dichroic mirrors for UV solid-state lasers," *Thin Solid Films*, vol. 517, no. 5, pp. 1731–1735, 2009.
- [14] A. Gatto *et al.*, "High-performance deep-ultraviolet optics for free-electron lasers," *Appl. Opt.*, vol. 41, no. 16, pp. 3236–3241, 2002.
- [15] P. Torchio, A. Gatto, M. Alvisi, G. Albrand, N. Kaiser, and C. Amra, "High-reflectivity HfO<sub>2</sub>/SiO<sub>2</sub> ultraviolet mirrors," *Appl. Opt.*, vol. 41, no. 16, pp. 3256–3261, 2002.
- [16] F. Réveret *et al.*, "High reflectance dielectric distributed Bragg reflectors for near ultra-violet planar microcavities: SiO<sub>2</sub>/HfO<sub>2</sub> versus SiO<sub>2</sub>/SiN<sub>x</sub>," *J. Appl. Phys.*, vol. 120, no. 9, Sep. 2016, Art. no. 093107.
- [17] E. Rauwel *et al.*, "Stabilization of the cubic phase of HfO<sub>2</sub> by Y addition in films grown by metal organic chemical vapor deposition," *Appl. Phys. Lett.*, vol. 89, no. 1, Jul. 2006, Art. no. 012902.
- [18] Z. K. Yang *et al.*, "Structural and compositional investigation of yttrium-doped HfO<sub>2</sub> films epitaxially grown on Si(111)," *Appl. Phys. Lett.*, vol. 91, no. 20, Nov. 2007, Art. no. 202909.
- [19] J. Y. Dai, P. F. Lee, K. H. Wong, H. L. W. Chan, and C. L. Choy, "Epitaxial growth of yttrium-stabilized HfO<sub>2</sub> high-k gate dielectric thin films on Si," *J. Appl. Phys.*, vol. 94, no. 2, pp. 912–915, 2003.
- [20] M. N.-A.-Alam, K. Abhilash, and C. V. Ramana, "Electrical and optical properties of nanocrystalline yttrium-doped hafnium oxide thin films," *Thin Solid Films*, vol. 520, no. 21, pp. 6631–6635, 2012.
- [21] X. Chen, L. Song, L. You, and L. Zhao, "Incorporation effect of Y<sub>2</sub>O<sub>3</sub> on the structure and optical properties of HfO<sub>2</sub> thin films," *Appl. Surf. Sci.*, vol. 271, pp. 248–252, 2013.
- [22] X. Chen *et al.*, "Effect of oxygen vacancies on the laser-induced damage resistance of Y<sub>0.26</sub>Hf<sub>0.74</sub>O<sub>x</sub> thin films," *Opt. Lett.*, vol. 39, no. 22, pp. 6470–6473, 2014.
- [23] L. Mohamed *et al.*, "Optical polarization control of photo-pumped stimulated emissions at 238 nm from AlGaIn multiple-quantum-well laser structures on AlN substrates," *Appl. Phys. Exp.*, vol. 10, no. 1, Jan. 2017, Art. no. 012702.
- [24] S. Zhao, X. Liu, Y. Wu, and Z. Mi, "An electrically pumped 239 nm AlGaIn nanowire laser operating at room temperature," *Appl. Phys. Lett.*, vol. 109, no. 19, Nov. 2016, Art. no. 191106.
- [25] X.-H. Li *et al.*, "Demonstration of transverse-magnetic deep-ultraviolet stimulated emission from AlGaIn multiple-quantum-well lasers grown on a sapphire substrate," *Appl. Phys. Lett.*, vol. 106, no. 4, Jan. 2015, Art. no. 041115.
- [26] Z. Lochner *et al.*, "Deep-ultraviolet lasing at 243 nm from photo-pumped AlGaIn/AlN heterostructure on AlN substrate," *Appl. Phys. Lett.*, vol. 102, no. 10, Mar. 2013, Art. no. 101110.
- [27] M. S. Alias *et al.*, "Optical constants of CH<sub>3</sub>NH<sub>3</sub>PbBr<sub>3</sub> perovskite thin films measured by spectroscopic ellipsometry," *Opt. Exp.*, vol. 24, no. 15, pp. 16586–16594, 2016.
- [28] G. E. Jellison and F. A. Modine, "Parameterization of the optical functions of amorphous materials in the interband region," *Appl. Phys. Lett.*, vol. 69, no. 3, pp. 371–373, 1996.
- [29] B. Deng *et al.*, "Modulation of the structural and optical properties of sputtering-derived HfO<sub>2</sub> films by deposition power," *Opt. Mater.*, vol. 37, pp. 245–250, 2014.
- [30] F. L. Martínez *et al.*, "Optical properties and structure of HfO<sub>2</sub> thin films grown by high pressure reactive sputtering," *J. Phys. D, Appl. Phys.*, vol. 40, no. 17, pp. 5256–5265, 2007.
- [31] J. M. Khoshman, A. Khan, and M. E. Kordesch, "Amorphous hafnium oxide thin films for antireflection optical coatings," *Surf. Coat. Technol.*, vol. 202, no. 11, pp. 2500–2502, 2008.
- [32] S. Jena *et al.*, "Effect of O<sub>2</sub>/Ar gas flow ratio on the optical properties and mechanical stress of sputtered HfO<sub>2</sub> thin films," *Thin Solid Films*, vol. 592, pp. 135–142, 2015.
- [33] G. H. Chen, Z. F. Hou, X. G. Gong, and Q. Li, "Effects of Y doping on the structural stability and defect properties of cubic HfO<sub>2</sub>," *J. Appl. Phys.*, vol. 104, no. 7, Oct. 2008, Art. no. 074101.
- [34] M. Ramzan *et al.*, "Optical characterization of hafnium oxide thin films for heat mirrors," *Mater. Sci. Semicond. Process.*, vol. 32, no. 5, pp. 22–30, 2015.
- [35] S. Heiroth, R. Ghisleni, T. Lippert, J. Michler, and A. Wokaun, "Optical and mechanical properties of amorphous and crystalline yttria-stabilized zirconia thin films prepared by pulsed laser deposition," *Acta Mater.*, vol. 59, no. 6, pp. 2330–2340, 2011.
- [36] A. Ortega, E. J. Rubio, K. Abhilash, and C. V. Ramana, "Correlation between phase and optical properties of yttrium-doped hafnium oxide nanocrystalline thin films," *Opt. Mater.*, vol. 35, no. 9, pp. 1728–1734, 2013.
- [37] H. Li and K. Iga, *Vertical-Cavity Surface-Emitting Laser Devices*. Berlin, Germany: Springer, 2003.
- [38] M. S. Alias, S. Shaari, and S. M. Mitani, "Optimization of electro-optical characteristics of GaAs-based oxide confinement VCSEL," *Laser Phys.*, vol. 20, no. 4, pp. 806–810, 2010.